in the inertial frame. Furthermore, we proposed a simple impedance controller to support the feet or hands to adapt to a low-friction ground without prior knowledge of the ground condition.

We experimentally validated our controller on a torque-controllable biped humanoid robot. The robot not only can adapt to unknown external forces applied to arbitrary contact points but to *unknown* time-varying terrain *without sensing* contact forces or terrain shape as well. A logical extension of this paper would be to enlarge the range of the terrain adaptability by foot placement [19], [20] with effective fusion of vision and contact information.

ACKNOWLEDGMENT

The author thanks Dr. G. Cheng and the anonymous reviewers for their helpful comments and suggestions.

REFERENCES

[1] J. Hollerbach and K. Suh, “Redundancy resolution of manipulators through torque optimization,” *IEEE J. Robot. Autom.*, vol. RA-3, no. 4, pp. 308–316, Aug. 1987.
[2] O. Khatib, “A unified approach for motion and force control of robot manipulators: The operational space formulation,” *IEEE J. Robot. Autom.*, vol. RA-3, no. 1, pp. 43–53, Feb. 1987.
[3] A. De Luca and G. Oriolo, “Issues in acceleration resolution of robot redundancy,” in *Proc. 3rd IFAC Symp. Robot. Control*, 1999, pp. 93–98.
[4] J. Pratt, C. Chew, A. Torres, P. Dilworth, and G. Pratt, “Virtual model control: An intuitive approach for bipedal locomotion,” *Int. J. Robot. Res.*, vol. 20, no. 2, pp. 129–143, 2001.
[5] L. Sentis and O. Khatib, “Synthesis of whole-body behaviors through hierarchical control of behavioral primitives,” *Int. J. Humanoid Robot.*, vol. 2, no. 4, pp. 505–518, 2005.
[6] R. M. Murray, Z. Li, and S. S. Sastry, *A Mathematical Introduction to Robotic Manipulation*. Boca Raton, FL: CRC, 1994.
[7] S. Hyon, J. G. Hale, and G. Cheng, “Full-body compliant human–humanoid interaction: Balancing in the presence of unknown external forces,” *IEEE Trans. Robot.*, vol. 23, no. 5, pp. 884–898, Oct. 2007.
[8] J. Yamaguchi, N. Kinoshita, A. Takanishi, and I. Kato, “Development of a dynamic biped walking system for humanoid development of a biped walking robot adapting to the humans’ living floor,” in *Proc. IEEE Int. Conf. Robot. Autom.*, 1996, vol. 1, pp. 232–239.
[9] K. Hirai, M. Hirose, Y. Haikawa, and T. Takenaka, “The development of the Honda humanoid robot,” in *Proc. IEEE Int. Conf. Robot. Autom.*, 1998, pp. 1321–1328.
[10] Y. Kuroki, M. Fujita, T. Ishida, K. Nagasaka, and J. Yamaguchi, “A small biped entertainment robot exploring attractive applications,” in *Proc. IEEE Int. Conf. Robot. Autom.*, 2003, pp. 471–476.
[11] M. Kawato, “From “understanding the brain by creating the brain” towards manipulative neuroscience,” *Philos. Trans. R. Soc.*, vol. 363, no. 1500, pp. 2201–2214, 2008.
[12] S. Hyon and G. Cheng, “Gravity compensation and full-body force interaction for humanoid robots,” in *Proc. IEEE-RAS Int. Conf. Humanoid Robots*, 2006, pp. 214–221.
[13] G. Cheng, S. Hyon, J. Morimoto, A. Ude, J. G. Hale, G. Colvin, W. Scroggin, and S. C. Jacobsen, “CB: A humanoid research platform for exploring neuroscience,” *Adv. Robot.*, vol. 21, no. 10, pp. 1097–1114, 2007.
[14] S. Arimoto, H. Hashiguchi, and R. Ozawa, “A simple control method coping with a kinematically ill-posed inverse problem of redundant robots: Analysis in case of a handwriting robot,” *Asian J. Control*, vol. 7, no. 2, pp. 112–123, 2005.
[15] C. Borst, C. Ott, T. Wimbock, B. Brunner, F. Zacharias, B. Bauml, U. Hillenbrand, S. Haddadin, A. Albu-Schaffer, and G. Hirzinger, “A humanoid upper body system for two-handed manipulation,” in *Proc. IEEE Int. Conf. Robot. Autom.*, 2007, pp. 2766–2767.
[16] H. Hirukawa, S. Hattori, S. Kajita, K. Harada, K. Kaneko, F. Kanehiro, M. Morisawa, and S. Nakaoka, “A pattern generator of humanoid robots walking on a rough terrain,” in *Proc. IEEE Int. Conf. Robot. Autom.*, 2007, pp. 2181–2187.
[17] N. Hogan, “Impedance control: An approach to manipulation: Parts I–III,” *Trans. ASME, J. Dyn. Syst., Meas., Control*, vol. 107, no. 1, pp. 1–24, 1985.
[18] S. Kajita, K. Kaneko, K. Harada, F. Kanehiro, K. Fujiwara, and H. Hirukawa, “Biped walking on a low friction floor,” in *Proc. IEEE/RSJ Int. Conf. Intell. Robots Syst.*, 2004, pp. 3546–3552.
[19] G. N. Boone and J. K. Hodgins, “Slipping and tripping reflexes for bipedal robots,” *Auton. Robots*, vol. 4, no. 3, pp. 259–271, 1997.
[20] S. Hyon and G. Cheng, “Disturbance rejection for biped humanoids,” in *Proc. IEEE Int. Conf. Robot. Autom.*, 2007, pp. 2668–2675.

Omnidirectional Visual-Servo of a Gough–Stewart Platform

O. Tahri, Y. Mezouar, N. Andreff, and P. Martinet

***Abstract*—This paper deals with the visual control of the Gough–Stewart platform using a central catadioptric camera observing the platform’s legs. This allows a large field of view to be obtained and avoids the occlusion problems observed when a classical perspective camera is used. An automatic and simple method to detect the projections of the leg in the image is also proposed. The control scheme presented here is shown to encompass the classical perspective camera case, as well as catadioptric ones. Finally, experimental results comparing two kinds of visual features (leg directions and leg edges) are described.**

***Index Terms*—Omnidirectional camera, parallel robots, visual servoing.**

I. INTRODUCTION

Most of the effort in visual servoing is devoted to serial robots, only a few studies have investigated the case of parallel mechanisms, while it has been shown in [2] that vision could be an interesting alternative to joint sensing for the following reasons:

1) Vision allows direct observation of the variables that are both relevant for kinematics and for control, namely the leg directions (which are crucial in the differential kinematic matrix, yielding a simpler solution to the forward kinematic problem) rather than the leg lengths.
2) Vision observes these directions, which are elements of the 3-D space, directly in their space and in a common reference frame for all legs, whereas joint sensing (namely, in the U-joints at the base) is an indirect observation in separate frames (one for each sensor).
3) Observation by vision reduces the kinematic parameter set, while joint sensing yields additional calibration or additional mechanical accuracy to position the joint sensing frames relative to each other.
4) Vision-based control is a sensor-based control, while joint-based control is a model-based control, which is inherently more sensitive to model errors.

The authors of [3] and [9]–[11] translated 3-D pose visual servoing techniques to parallel mechanisms using standard kinematic models. More recently, three kinds of features have been proposed for visual servoing of parallel mechanisms [1], [2], [7]. The end-effector pose in [7] is measured by vision and used for regulation. However, the

Manuscript received April 30, 2008; revised September 22, 2008. First published January 6, 2009; current version published February 4, 2009. This paper was recommended for publication by Associate Editor F. Thomas and Editor F. Park upon evaluation of the reviewers’ comments. This paper was presented in part at the IEEE/RSJ International Conference on Intelligent Robots and Systems, San Diego, CA, 2007.

The authors are with LASMEA, Blaise Pascal University, 63177 Aubière, France (e-mail: tahri@univ-bpclermont.fr; mezouar@univ-bpclermont.fr; andreff@univ-bpclermont.fr; martinet@univ-bpclermont.fr).

Color versions of one or more of the figures in this paper are available online at http://ieeexplore.ieee.org.

Digital Object Identifier 10.1109/TRO.2008.2008745

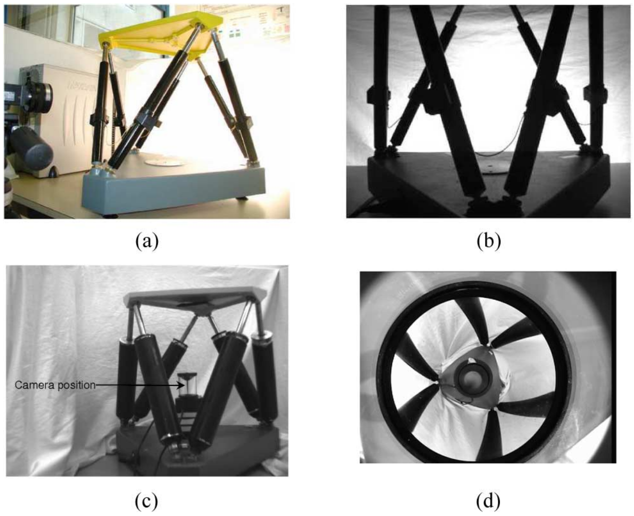

Fig. 1. Gough–Stewart platform observed by a classical perspective camera. (a) Camera position with respect to the platform and (b) image of the legs. A Gough–Stewart platform observed by an omnidirectional camera. (c) Camera position with respect to the platform and (d) image of the legs.

direct application of visual servoing techniques assumes implicitly that the robot inverse differential kinematic model is given and that it is calibrated. Therefore, [1] and [2] propose, respectively, image-based and position-based visual-servo schemes by directly observing the platform legs with a classical perspective camera. Unfortunately, to position adequately the camera to observe simultaneously all the platform legs is a complex task. The camera was positioned in [1] and [2] in front of the platform [see Fig. 1(a)]. In this case, the legs in front of the platform are closer to the camera than the ones in the back. As a consequence, the extraction of the image features lying on legs in the back will be less robust. Furthermore, large parts of the legs in the back are occluded by the front legs [see Fig. 1(b)] and full occlusions can happen. This is an important drawback since the vision-based control assumes that all legs can be observed during the servoing task. A first solution to address this issue could be to employ a system made of multiple cameras. However, in this case, data provided by each camera must be synchronized and the multicamera system calibrated. A second and simpler solution, whose first results were presented in [14], consists of positioning a single omnidirectional camera (vision system providing 360° panoramic views of the scene) at the platform center [see Fig. 1(c)]. This way, all the legs can be simultaneously observed in a panoramic view, and potential occlusions cannot occur [see Fig. 1(d)]. Moreover, by positionning the omnidirectional camera at the platform center, the feature extraction should be more robust than when a conventional camera is employed since the legs will be closer to the image plane. Finally, observing legs, even using an omnidirectional camera allows a linear calibration of the platform [6]. Clearly, visual servoing of the Gough–Stewart platform will benefit from the enhanced field of view provided by an omnidirectional camera. However, omnidirectional images exhibit supplementary difficulties compared with conventional perspective image (for example, the projection of a line is no more a line but a conic curve). In this paper, we propose to use the unified model described in [8], since it allows to formulate control laws that are valid for any sensor obeying the unified camera model. In other words, it encompasses all sensors in this class [8], [13]: perspective and catadioptric. Some classes of fisheye cameras are also covered by this model [5], [13].

Parallel robots are supposedly capable of realizing a large displacement in a limited period of time. Thus, the motion of the legs projection

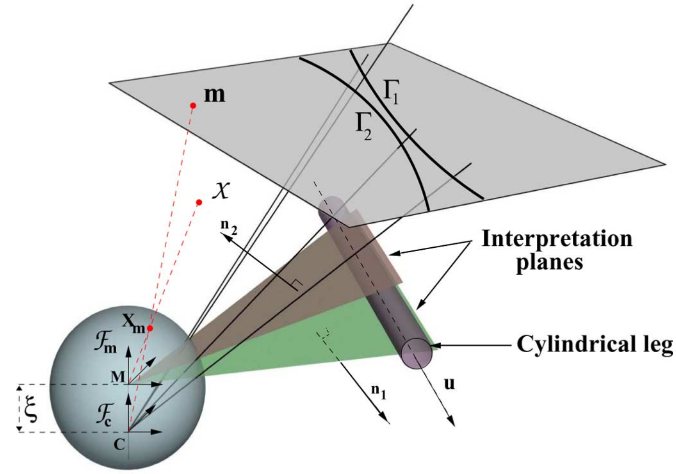

Fig. 2. Projection of a cylindrical leg onto the image plane.

in the image could be very large. At this level, tracking algorithms based on iterative minimization (refer for example to [4] and [12] for algortihm dedicated to omnidirectional images) might break down. To overcome these problems, we propose an automatic detection of the platform legs from an omnidirectional image which is thus suitable for high-speed tasks. Further, control laws obtained using legs orientation and the legs interpretation planes with perspective camera are extended to the case of omnidirectional camera. Experimental results comparing two kinds of visual features (leg directions and leg edges) and control laws in perspective and omnidirectional cases are also described.

In the next section, a camera model, cylindrical leg observation, and control laws are recalled. In Section III, an automatic leg detection in the image is proposed and exploited to robustly estimate the visual features. Section IV is dedicated to experimental results.

II. Modeling and Control

A. Camera Model

Central imaging systems can be modeled using two consecutive projections: spherical projection and then perspective one. This geometric formulation called unified model has been proposed by Geyer and Daniilidis in [8] and has been intensively used by the vision and robotics community (structure from motion, calibration, visual servoing, etc.). Let us outline the essentials of this model. Consider a virtual unitary sphere centered in M, as shown in Fig. 2, and the perspective camera centered in C. The frames attached to the sphere and the perspective camera are related by a simple translation of $-\xi$ along the Z-axis. Let $\mathcal{X}$ be a 3-D point with coordinates $\mathbf{X} = [X\ Y\ Z]^\top$ in $\mathcal{F}_m$. The world point $\mathcal{X}$ is projected in the image plane into the point of homogeneous coordinates $\mathbf{p} = \mathbf{K}\mathbf{m}$, where $\mathbf{K}$ is a 3×3 upper triangular matrix containing the conventional camera-intrinsic parameters coupled with mirror-intrinsic parameters and

$$\mathbf{m} = [x\ y\ 1]^\top = \left[\frac{X}{Z + \xi\|\mathbf{X}\|} \quad \frac{Y}{Z + \xi\|\mathbf{X}\|} \quad 1\right]^\top \tag{1}$$

The matrix $\mathbf{K}$ and the parameter ξ can be obtained after calibration using, for example, the methods proposed in [13]. In the sequel, the central imaging system is considered calibrated. In this case, the inverse projection onto the unit sphere $\mathbf{X_m}$ can be obtained as

$$\mathbf{X_m} = \lambda \left[x\ y\ 1 - \frac{\xi}{\lambda}\right]^\top \tag{2}$$

where $\lambda = \frac{\xi + \sqrt{1+(1-\xi^2)(x^2+y^2)}}{x^2+y^2+1}$.

B. Cylindrical Leg Observation

A Gough–Stewart platform has six cylindrical legs of varying length q_j $(j = 1, \ldots, 6)$ attached to the base by spherical joints located at points $\mathbf{A}_j$, and to the moving platform by spherical joints located at points $\mathbf{B}_j$ (see Fig. 1). The image of the jth leg is defined by the projection onto the image plane of two lines ($\mathcal{L}_1^j$ and $\mathcal{L}_2^j$), as depicted in Fig. 2. Let $\mathbf{n}_j^i = [n_{jx}^i \; n_{jx}^i \; n_{jx}^i]^\top$ $(i = 1,\, 2)$ be the unitary vector orthogonal to the interpretation plane π_j^i defined by the line $\mathcal{L}_j^i$ and the projection center. The points $\mathbf{X}_m$ lying on the intersection between π_j^i and the sphere are then defined by

$$\begin{cases} \|\mathbf{X}_m\| = 1 \\ \mathbf{n}_j^{i\top} \mathbf{X}_m = 0. \end{cases} \tag{3}$$

Using the spherical coordinates given by (2), it can be shown that 3-D points lying on $\mathcal{L}_j^i$ are mapped onto points $\mathbf{m}$ lying on a conic curve Γ_j^i, which can be written as

$$\alpha_0 x^2 + \alpha_1 y^2 + 2\alpha_2 xy + 2\alpha_3 x + 2\alpha_4 y + \alpha_5 = 0 \tag{4}$$

where $\alpha_0 = n_{jx}^{i2} - \xi^2(1 - n_{jy}^{i2})$, $\alpha_1 = n_{jy}^{i2} - \xi^2(1 - n_{jx}^{i2})$, $\alpha_2 = n_{jx}^i n_{jy}^i (1 - \xi^2)$, $\alpha_3 = n_{jx}^i n_{jz}^i$, $\alpha_4 = n_{jy}^i n_{jz}^i$, and $\alpha_5 = n_{jz}^{i2}$. Let us note that (4) is defined up to a scale factor. If $\alpha_5 \neq 0$, the number of parameters can be reduced to

$$\beta_0 x^2 + \beta_1 y^2 + 2\beta_2 xy + 2\beta_3 x + 2\beta_4 y + 1 = 0 \tag{5}$$

with $\beta_k = \frac{\alpha_k}{\alpha_5}$. From the parameters β_k, it is possible to determine the perpendicular vector to the interpretation plane as follows:

$$n_{jz}^i = (\beta_3^2 + \beta_4^2 + 1)^{-\frac{1}{2}}, \quad n_{jx}^i = \beta_3\, n_{jz}^i, \quad n_{jy}^i = \beta_4\, n_{jz}^i. \tag{6}$$

The case where $\alpha_5 = 0$ corresponds to a degenerate configuration where the optical axis lies on the interpretation plane. Unfortunately this happens for several end-effector poses in our application. Therefore, the estimation of $\mathbf{n}_j^i$ using (6) will not be suitable, since $\alpha_3 = \alpha_4 = \alpha_5 = 0$. For this reason, a more robust estimation of $\mathbf{n}_j^i$ from the projection onto a sphere will be proposed in the following portions of this paper. The orientation of the jth leg, which is expressed in the camera frame, can straightforwardly be computed from the related normal vectors

$$\mathbf{u}_j = \frac{\mathbf{n}_j^1 \times \mathbf{n}_j^2}{\|\mathbf{n}_j^1 \times \mathbf{n}_j^2\|}. \tag{7}$$

C. Control

In few words, let us recall that the time variation $\dot{\mathbf{s}}$ of the visual features $\mathbf{s}$ can be expressed linearly with respect to the relative camera–object kinematic twist $\mathbf{v}$ by $\dot{\mathbf{s}} = \mathbf{L_s}\mathbf{v}$, where $\mathbf{L_s}$ is the interaction matrix related to $\mathbf{s}$. The exponential decay of $\mathbf{s} - \mathbf{s}^*$ ($\mathbf{s}^*$ being the desired value of $\mathbf{s}$) can be obtained using the following control law:

$$\mathbf{v} = -\lambda\, \widehat{\mathbf{L_s}}^{+} (\mathbf{s} - \mathbf{s}^*) \tag{8}$$

where $\widehat{\mathbf{L_s}}$ is a model or an approximation of $\mathbf{L_s}$, $\widehat{\mathbf{L_s}}^{+}$ the pseudoinverse of $\widehat{\mathbf{L_s}}$, and λ a positive gain tuning the time to convergence.

1) Visual Servoing of Leg Directions: To servo the leg directions, we define $\mathbf{s}$ as the geodesic error between the current leg orientation $\mathbf{u}_j$ and the desired one $\mathbf{u}_j^*$

$$\mathbf{s}_{\mathbf{u}j} = \mathbf{u}_j \times \mathbf{u}_j^*,\; j = 1, \ldots, 6. \tag{9}$$

This means that $\mathbf{s}_{\mathbf{u}_j}^* = \mathbf{0}_{3\times 1}, j = 1, \ldots, 6$. Following [2], the interaction matrix associated with a leg orientation $\mathbf{u}_j$ is

$$\dot{\mathbf{u}}_j = \mathbf{M}_j\, \mathbf{v} \tag{10}$$

$$\mathbf{M}_j = -\frac{1}{q_j}\left[\mathbf{I}_3 - \mathbf{u}_j \mathbf{u}_j^\top\right]\left[\mathbf{I}_3 \quad -[\mathbf{A}_j + q_j \mathbf{u}_j]_\times\right]. \tag{11}$$

By combining (9) and (10), we obtain

$$\dot{\mathbf{s}}_{\mathbf{u_j}} = \mathbf{L}_{\mathbf{u_j}}\, \mathbf{v} \tag{12}$$

$$\mathbf{L}_{\mathbf{u_j}} = -[\mathbf{u}_j^*]_\times \mathbf{M}_j. \tag{13}$$

Now, the standard method applies. We stack each individual error $\mathbf{s}_{\mathbf{u_j}}$ in a single overconstrained vector $\mathbf{s_u}$ as well as each associated individual interaction matrix $\mathbf{L}_{\mathbf{u_j}}$ into a compound one $\mathbf{L}_u$ and impose a first-order convergence to $\mathbf{s_u}$. Finally, the control law (8) is used for the platform positioning.

2) Visual Servoing of the Interpretation Planes: Another possible set of visual features to control the Gough–Steward platform is composed of the two edges of each cylinder leg. Contrary to the perspective case where the leg edge projection is a line (and can be represented by a simple change of coordinates of the interpretation plane), the general case requires to reconstruct the interpretation planes in the frame related to the sphere (i.e., the sphere defined in the camera-unified model) from the image data, knowing the intrinsic parameters. More details about the interpretation planes reconstruction in the general case is given in [14]. Formally, the features related to the interpretation planes are defined by

$$\mathbf{s}_{\mathbf{n_j^i}} = \mathbf{n}_j^i \times \mathbf{n}_j^{i*}, \qquad j = 1, \ldots, 6,\; i = 1, 2. \tag{14}$$

The derivative of a leg edge expressed in the camera frame can be obtained as described in [1]

$$\dot{\mathbf{n}}_j^i = {}^{\mathbf{n}}\mathbf{J_u} \mathbf{M}_i \mathbf{v} \tag{15}$$

$${}^{\mathbf{n}}\mathbf{J_u} = \left[\frac{(\mathbf{u}_j \times \mathbf{n}_j^i)\mathbf{A}_j^\top}{\mathbf{A}_j(\mathbf{u}_j \times \mathbf{n}_j^i)^\top} - \mathbf{I}\right] \mathbf{u}_j \mathbf{n}_j^{i\top}. \tag{16}$$

Consequently, by combining (14) and (16), the time derivative of $\mathbf{s}_{\mathbf{n_j^i}}$ can be written as

$$\dot{\mathbf{s}}_{\mathbf{n_j^i}} = \mathbf{L}_{\mathbf{n_j^i}}\, \mathbf{v} \tag{17}$$

$$\mathbf{L}_{\mathbf{n_j^i}} = -[\mathbf{n}_j^{i*}]_\times\, {}^{\mathbf{n}}\mathbf{J_u} \mathbf{M}_i. \tag{18}$$

III. Image Processing and Estimations

A. Fast and Automatic Detection of the Platform Legs in Image

The region beneath the end-effector and between the legs is completely separated from the workspace. For this reason, a white background is used to facilitate the leg detection. Furthermore, the projection of the legs in the image is almost radial [see Fig. 3(a)]. This property is used to develop a fully automatic detection algorithm. A set of circles centered on the principal point with diameters ranging from a minimal value $d_{\min}$ to a maximal value $d_{\max}$ is first defined. As we can see in Fig. 3(a), $d_{\min}$ and $d_{\max}$ and the circle center are fixed such that only the image part, where the legs are projected, is under consideration. Next, the image is scanned along each circle providing a monodimensional signal [see Fig. 3(b)] that is then thresholded to obtain a binary signal [see Fig. 3(c)]. The peaks of the signal derivative are obtained using a gradient filter [see Fig. 3(d)]. The peaks of the signal provide then the image of the leg limbs. It is possible to detect the peaks from

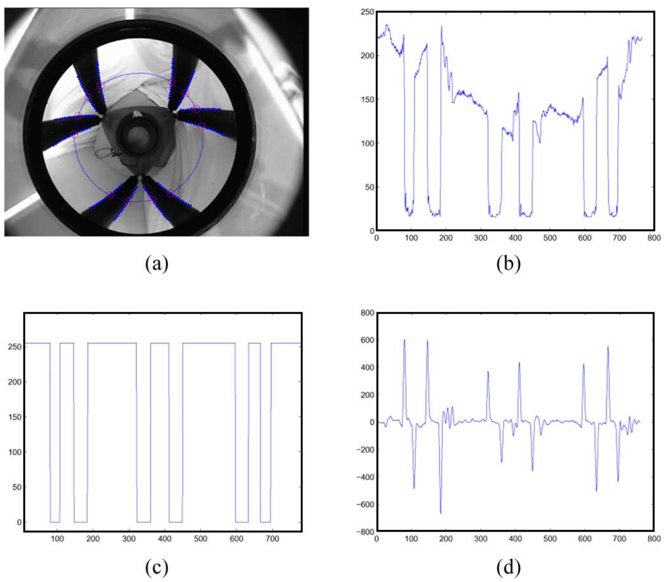

Fig. 3. Automatic detection of legs in the image. (a) Detection principle, (b) monodimensional signal along the defined circle, (c) signal along the defined circle after thresholding, and (d) the derivative of the obtained signal after thresholding.

the derivative of the signal without the thresholding step. However, in this case, unexpected peeks appear. The thresholding step has got to avoid them and make the detection of the peaks belonging to the platform legs easier.

In theory, two circles are enough to determine each leg's edges in the image. In practice, more than two image points of each edge are required to obtain a robust estimation. For our experiments, a set of 17 circles (which is a good compromise between robustness and time) with $d_{\min} = 184$ pixel and $d_{\max} = 370$ pixel is defined. Finally, note that the proposed method is fully automatic (no initialization by the user is required) and that less than 0.3 ms is necessary to detect the leg edges with a conventional labtop.

B. Estimation of Leg Orientations and Their Related Interaction Matrices

Assume now that the image points belonging to the leg's edges have been extracted using the method described previously and that the corresponding points in the normalized plane have been estimated knowing the camera parameters. The perpendicular vector to the interpretation plane $\mathbf{n}$ can then be computed in two ways: 1) The conic's parameters β_k are first linearly estimated using (5) and then exploited to compute $\mathbf{n}$ from (6); 2) the point on the sphere is first estimated from the point coordinates in the normalized plane using (2), and then, $\mathbf{n}$ is linearly estimated using (3). In practice, the second method gives more robust results with respect to noise. This is expected since the first method uses a set of nonminimal parameters (five parameters instead of only two independent ones), while the second one uses a set of minimal parameters in a linear optimization procedure. Once the perpendicular vectors to the two leg edges are computed, the corresponding leg orientations can be computed from (7). From (10), we note that the interaction matrix depends on the leg orientation, the attachment points $\mathbf{A_j}$ expressed in the camera frame, the articulation value q_j, and the leg's orientation vector itself. The joint values q_j appear two times in (10): under the form $[\mathbf{A}_j + q_j\, {}^c\underline{\mathbf{u}}]_\times$ and as a gain. Considering the order of magnitude of $\mathbf{A_j}$ and q_j, one can neglect small

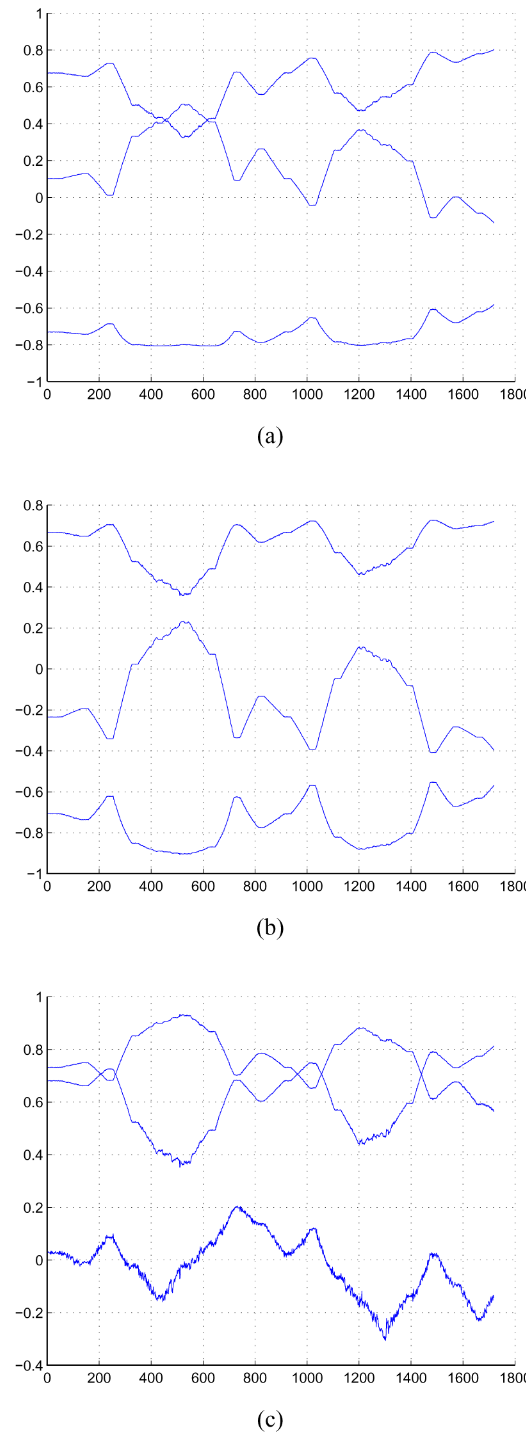

Fig. 4. Sensitivity of estimation. (a) Three components of the normal vector to the interpretation plane of the first limb (unitless), (b) the three components of the normal vector to the interpretation plane of the second limb, and (c) the three components of direction vector of the first leg.

errors in the joint offsets. Moreover, since the joints are prismatic, it is easy to measure their offsets manually with millimetric accuracy. This is also sufficient to ensure that the gain is accurate enough. Now, to totally determine the interaction matrices, the attachment points $\mathbf{A_j}$ have to be computed. In [6], a calibration procedure was proposed, using leg observation. This method can be combined with the automatic leg detection to make it more practical.

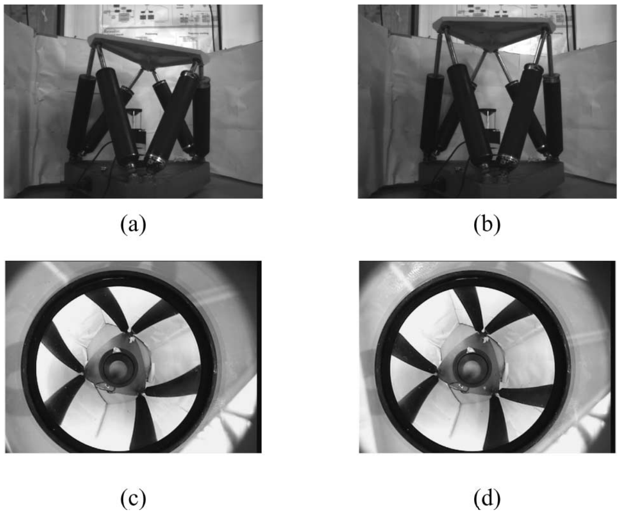

Fig. 5. Experimental results. (a) Initial configuration, (b) desired configuration, (c) initial image, and (d) desired image.

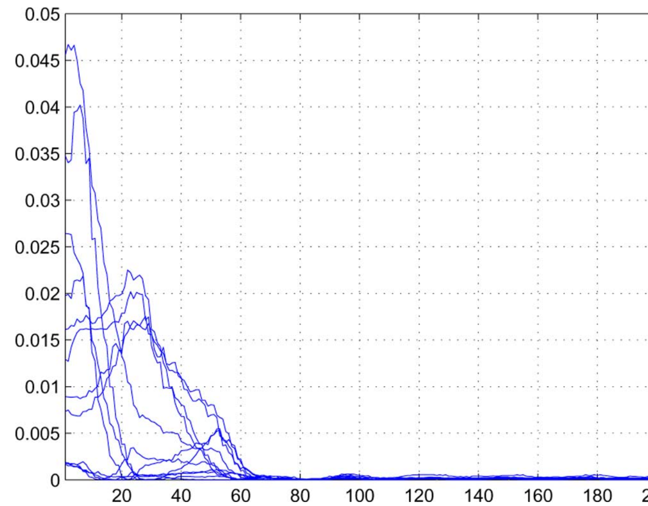

Fig. 6. Errors $\mathbf{s}_{\mathbf{n}_j}\mathbf{s}_{\mathbf{n}_j}^{\top}$ (unitless) using the leg edges ($\mathbf{s}_{\mathbf{n}_j}$) as visual features with respect to time.

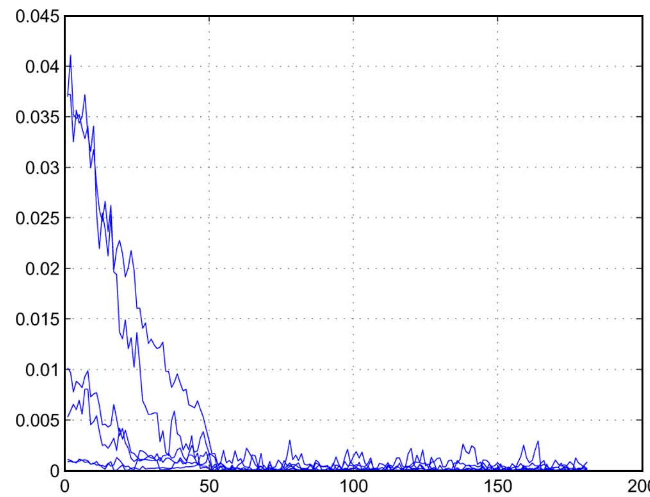

(a)

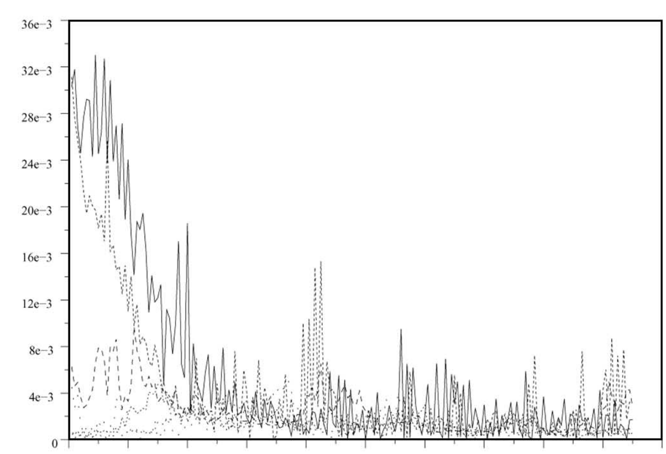

(b)

Fig. 7. Experimental results using leg orientations ($\mathbf{s}_{\mathbf{u}_j}$). Errors $\mathbf{s}_{\mathbf{u}_j}\mathbf{s}_{\mathbf{u}_j}^{\top}$ (unitless) (a) using an omnidirectional camera and (b) using a conventional camera (presented in [1]) with respect to time (expressed as iteration number).

IV. Experimental Results

The proposed approach has been validated on the commercial DeltaLab *Table de Stewart* shown in Fig. 5. The legs of the platform have been modified to improve image processing. The experimental robot has an analog joint position controller interfaced with Linux-RTAI.Joint velocity control is emulated through this position controller with an approximate 20-ms sampling period. The omnidirectional camera used is a parabolic mirror combined with an orthographic lens. It is approximately placed at the base center.

A. Robustness of Estimation

In a first experiment, a sequence of end-effector poses was performed by the robot. Further, nearly 1700 images were acquired while the robot was moving between the various poses in order to get a smooth leg's edges.For each image of the platform legs, the corresponding perpendicular vector to the interpretation planes as well as the direction vector of the legs in the camera frame were computed. Fig. 4 shows the estimation results obtained for one robot leg (the results for the other legs are similar). First, Fig. 4(a) and (b) give the entries of the perpendicular vector to the interpretation plane of the two leg edges. From these figures, we note that the variation of vector entries for the image sequence is very smooth. This shows that the detection method, as well as the estimation method of the vectors $\mathbf{n}$ used in this paper, are particulary robust. On the other hand, Fig. 4(c) shows the variation of the entries of the leg direction vector for the same image sequence. From this figure, the variation of the vector entries is still smooth but noisier compared with the results obtained for the perpendicular vectors to the interpretation planes for the same leg.

B. Visual Servo of the Gough–Stewart Platform

In the following experiments, we give an example of an omnidirectional visual servo of the Gough–Stewart platform. The initial and desired configurations of the platform are given, respectively, on Figs. 5(a) and (b). The corresponding images are given, respectively, on 5(c) and (d). In a first experiment, the leg directions were used to control the end-effector pose. Fig. 7(a) gives the behavior of the feature error squares $\mathbf{s}_\mathbf{i}{}^{\top}\mathbf{s}_\mathbf{i}$. From this figure, we note that these errors decrease to 0. Furthermore, the obtained plots are smoother than the results obtained

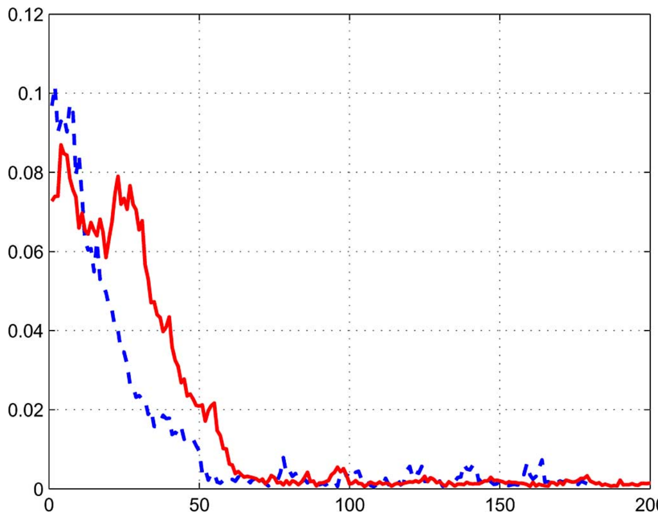

Fig. 8. Evolution of leg orientations during the control (sum of norms of the errors $\sum_{j=1}^{j=6} \|\mathbf{s}_{\mathbf{u_j}} \mathbf{s}_{\mathbf{u_j}}^{\top}\|$) with respect to time. Results using leg orientation (dashed plot), and results using leg edges (continuous plot).

using a conventional perspective camera reported in [1] [see Fig. 7(b)]. This is expected, since the omnidirectional cameras allow for the full observation of the robot legs. Furthermore, the latter are closer to the image plane than in the case where a conventional camera is used. Last, the edges detection is more robust.

In a second experiment and for the same initial and desired robot configurations, the leg edges were used to control the end-effector pose. The same scalar gain λ was used for the first and second experiments. Fig. 6 shows that the system converges. However, plots of the feature errors are clearly smoother and less noisy than in Fig. 7(a). This was expected, since the estimation of the leg orientation is less robust than the estimation of the perpendicular vectors to the interpretation planes, as was shown in Section IV-A. Furthermore, Fig. 8 gives the plot of the variations of the leg orientation using leg orientation or leg edges as features in the control law. From this figure, it can be noticed that the variation of the orientation using leg edges (dashed plot) in the control is smoother and less noisy than using leg orientations (continuous plot).

Concerning the stability, it is well known that if the interaction matrix is full rank then the classical (asymptotic) convergence condition holds, i.e., $\mathbf{L}\widehat{\mathbf{L}}^{+} > 0$. From this condition it is clear that if the interaction matrix can be perfectly measured, then the convergence is ensured since $\mathbf{L}\widehat{\mathbf{L}}^{+} = \mathbf{I}$. Note that only local (asymptotic) convergence is achieved when the interaction matrix of the desired configuration is used in the control law. However, when the interaction matrix cannot be perfectly measured (measurement noise, calibration errors, and errors in 3-D information), then the analysis of the convergence condition $\mathbf{L}\widehat{\mathbf{L}}^{+} > 0$ is an open problem (in the case of catadioptric camera as well as in the case of conventional camera). Now, we are concerned with the statistical studies of the convergence rate using both leg's orientation or leg's edges. In this way, 10 000 of random poses for the current and the desired positions of the platform have been generated using a robot simulator. However, only those poses where the leg's length belong to a defined interval $[q_{\min}\ q_{\max}]$ are allowed. These limits correspond to the joint limits of our real Gough–Stewart Platform. The convergence percentage (the percentage of the case where the platform has reached the desired position) is computed using each feature. In the ideal case (no calibration errors), the percentage of the convergence success among 10 000 different tests generated was 100% using the two kinds of features.

V. Conclusion

To date, and as far as we know, there is no study coupling the use of the central catadioptric camera and parallel robots control. The use of an omnidirectional camera allows the observation of all the platform legs without any occlusion. Furthermore, the leg positions with respect to the image plane make their detection by a fully automatic method very easy. No initialization of the leg positions in image is required. From the leg projections onto catadioptric plane, the interpretation plane vectors corresponding to leg edges, as well as the leg orientations, could easily be determined. Experimental results comparing the control behavior using each one of the latter features were given, showing that we can, expect better results using leg edges than with leg directions.

References

[1] N. Andreff, T. Dallej, and P. Martinet, "Image-based visual servoing of a Gough–Stewart parallel manipulator using leg observations," *Int. J. Robot. Res.*, vol. 26, no. 7, pp. 677–687, 2007.

[2] N. Andreff and P. Martinet, "Unifying kinematic modeling, identification and control of a Gough-Stewart parallel robot into a vision-based framework," *IEEE Trans. Robot.*, vol. 22, no. 6, pp. 1077–1086, Dec. 2006.

[3] L. Angel, J. M Sebastian, A Traslosheros, F. Roberti, and R. Carelli, "Visual servoing of a parallel robot system," in *Proc. Eur. Control Conf., (ECC 2007)*, Kos, Greece, Jul., pp. 1463–1470.

[4] F. M. J. Barreto and R. Horaud, "Visual servoing/tracking using central catadioptric cameras," presented at the Int. Symp. Exp. Robot., Adv. Robot. Ser., P. Dario and B. Siciliano, Eds. Berlin, Germany: Springer-Verlag, Jul. 2002.

[5] J. Courbon, Y. Mezouar, L. Eck, and P. Martinet, "A generic fisheye camera model for robotic applications," in *Proc. IEEE/RSJ Int. Conf. Intell. Robots Syst.*, San Diego, CA, Oct. 29–Nov. 2, 2007, pp. 1683–1688.

[6] T. Dallej, H. H. Abdelkader, N. Andreff, and P. Martinet, "Kinematic calibration of a Gough–Stewart platform using an omnidirectional camera," in *Proc. IEEE/RSJ Int. Conf. Intell. Robots Syst. (IROS 2006)*, Beijing, China, May, pp. 4666–4671.

[7] T. Dallej, N. Andreff, Y. Mezouar, and P. Martinet, "3d pose visual servoing relieves parallel robot control from joint sensing," in *Proc. IEEE/RSJ Int. Conf. Intell. Robots Syst. (IROS 2006)*, Beijing, China, Oct., pp. 4291–4296.

[8] C. Geyer and K. Daniilidis, "Mirrors in motion: Epipolar geometry and motion estimation," *Int. J. Comput. Vis.*, vol. 45, no. 3, pp. 766–773, 2003.

[9] P. Kallio, Q. Zhou, and H. N. Koivo, "Three-dimensional position control of a parallel micromanipulator using visual servoing," in *Proc. SPIE, Microrobot. Microassem. II*, B. J. Nelson and J.-M. Breguet, Eds. Boston, MA, Nov. 2000, vol. 4194, pp. 103–111.

[10] H. Kino, C. C. Cheah, S. Yabe, S. Kawamua, and S. Arimoto, "A motion control scheme in task oriented coordinates and its robustness for parallel wire driven systems," in *Proc. Int. Conf. Adv. Robot. (ICAR 1999)*, Tokyo, Japan, Oct., pp. 545–550.

[11] M. L. Koreichi, S. Babaci, F. Chaumette, G. Fried, and J. Pontnau, "Visual servo control of a parallel manipulator for assembly tasks," in *Proc. 6th Int. Symp. Intell. Robot. Syst. (SIRS 1998)*, Edinburgh, U.K., Jul., pp. 109–116.

[12] E. Marchand and F. Chaumette, "Fitting 3d models on central catadioptric images," in *Proc. IEEE Int. Conf. Robot. Autom.*, Rome, Italy, Apr. 2007, pp. 52–58.

[13] C. Mei and P. Rives, "Single view point omnidirectional camera calibration from planar grids," in *Proc. IEEE Int. Conf. Robot. Autom.*, Rome, Italy, Apr. 2007, pp. 3945–3950.

[14] O. Tahri, Y. Mezouar, N. Andreff, and P. Martinet, "Omnidirectional visual-servo of a Gough–Stewart platform," in *Proc. IEEE/RSJ Int. Conf. Intell. Robots Syst.*, San Diego, CA, Oct. 29–Nov. 2, 2007, pp. 1326–1331.